Physics Letters B 820 (2021) 136550

Contents lists available at ScienceDirect

Physics Letters B

www.elsevier.com/locate/physletb

Stationary solutions for fast flavor oscillations of a homogeneous dense neutrino gas

Zewei Xiong [a,b,*], Yong-Zhong Qian [a]

[a] School of Physics and Astronomy, University of Minnesota, Minneapolis, MN 55455, USA
[b] GSI Helmholtzzentrum für Schwerioneneforschung, 64291 Darmstadt, Germany

ARTICLE INFO

Article history:
Received 12 April 2021
Received in revised form 5 June 2021
Accepted 22 July 2021
Available online 24 July 2021
Editor: W. Haxton

Keywords:
Neutrino oscillations
Dense neutrino gas
Fast flavor oscillations

ABSTRACT

We present a method to find the stationary solutions for fast flavor oscillations of a homogeneous dense neutrino gas. These solutions correspond to collective precession of all neutrino polarization vectors around a fixed axis in the flavor space on average, and are conveniently studied in the co-rotating frame. We show that these solutions can account for the numerical results of explicit evolution calculations, and that even with the simplest assumption of adiabatic evolution, they can provide the average survival probabilities to good approximation. We also discuss improvement of these solutions and their use as estimates of the effects of fast oscillations in astrophysical environments.

1. Introduction

Experiments with solar, atmospheric, reactor, and accelerator neutrinos have established that neutrinos produced in a specific flavor state oscillate among all three flavor states [1]. Neutrino oscillations studied by the above experiments depend on the vacuum neutrino mixing properties and forward neutrino-electron scattering in the relevant matter. Because flavor evolution of individual neutrinos can be treated separately in these cases, the theory is well understood and calculations are straightforward. In astrophysical environments such as supernovae and neutron star mergers, however, neutrino emission is so intense that forward scattering among neutrinos becomes important, which causes flavor evolution to be coupled for neutrinos emitted with different energies and directions. Consequently, collective flavor oscillations (see e.g., [2] for a review of the early studies) may occur for the dense neutrino gas in these environments. The treatment and understanding of such oscillations are still evolving and under intensive study (see e.g., [3–8] for some recent developments).

Many insights can be obtained by studying oscillations of astrophysical neutrinos in terms of mixing between ν_e and ν_x, which represents an appropriate linear combination of ν_μ and ν_τ. In this case, the flavor field can be conveniently described by the polarization vector $\mathsf{P}(\omega, \mathbf{v})$ for a neutrino (antineutrino) emitted with energy E and velocity $\mathbf{v}$. Here $\omega = \pm\delta m^2/(2E)$ is the vacuum oscillation frequency, $\delta m^2 > 0$ is the mass-squared difference between the two vacuum mass eigenstates, and $\omega > 0$ ($\omega < 0$) denotes neutrinos (antineutrinos). For clarity, the sans serif font and numeral indices are used for quantities in the flavor space, while the bold face and (x, y, z) indices are used for vectors in the Euclidean space. The probability of being the electron flavor is $(P_3 + 1)/2$, where $P_3 = \mathsf{P} \cdot \hat{\mathsf{e}}_3$ and $\hat{\mathsf{e}}_3$ is the unit vector in the third direction of the flavor space. For coherent flavor evolution (i.e., in the absence of collisions) that starts with all neutrinos in pure flavor states, the $\mathsf{P}(\omega, \mathbf{v})$ for the initial ν_e and ν_x ($\bar{\nu}_e$ and $\bar{\nu}_x$) will differ only by an overall sign. Hereafter, $\mathsf{P}(\omega, \mathbf{v})$ specifically refers to the polarization vector of the initial ν_e or $\bar{\nu}_e$.

The general equation governing the spatial and temporal evolution of $\mathsf{P}(\omega, \mathbf{v})$ is

$$(\partial_t + \mathbf{v} \cdot \nabla)\mathsf{P}(\omega, \mathbf{v}) = \mathsf{H}(\omega, \mathbf{v}) \times \mathsf{P}(\omega, \mathbf{v}), \tag{1}$$

where $\mathsf{H}(\omega, \mathbf{v}) = \mathsf{H}_{\rm vac}(\omega) + \mathsf{H}_{\rm mat} + \mathsf{H}_{\nu\nu}(\mathbf{v})$ is the total Hamiltonian. The term $\mathsf{H}_{\rm vac}(\omega) = \omega\mathsf{B}$ accounts for the vacuum mixing, where $\mathsf{B} = (\sin 2\theta_V, 0, -\cos 2\theta_V)$ for the normal mass hierarchy and $\mathsf{B} = (-\sin 2\theta_V, 0, \cos 2\theta_V)$ for the inverted mass hierarchy with θ_V being the vacuum mixing angle. The contribution $\mathsf{H}_{\rm mat} = \lambda\hat{\mathsf{e}}_3$ originates from forward neutrino-electron scattering, where $\lambda = \sqrt{2}G_F n_e$, G_F is the Fermi coupling constant, and n_e is the net electron number density. The contribution $\mathsf{H}_{\nu\nu}(\mathbf{v})$ from forward scattering among neutrinos is our main concern and is discussed below.

We write $\mathsf{H}_{\nu\nu}(\mathbf{v}) = v^\rho(\mathbf{v})\mathsf{J}_\rho$, where $v^\rho(\mathbf{v}) = (1, \mathbf{v})$ is the four-vector corresponding to $\mathbf{v}$ with ρ running over (t, x, y, z),

* Corresponding author.
E-mail address: z.xiong@gsi.de (Z. Xiong).

https://doi.org/10.1016/j.physletb.2021.136550

$$\mathsf{J}^\rho = \mu \int d\mathbf{v}'\, v^\rho(\mathbf{v}') \int_{-\infty}^{+\infty} d\omega\, G(\omega,\mathbf{v}')\mathsf{P}(\omega,\mathbf{v}') \tag{2}$$

is the neutrino polarization current, $\mu = \sqrt{2}G_F n_{\nu_e}$, $n_{\nu_e} = \int d\mathbf{v} \int_0^\infty d\omega\, F_{\nu_e}(\omega,\mathbf{v})$ is the ν_e number density, $F_{\nu_e}(\omega,\mathbf{v})$ with $\omega > 0$ ($\omega < 0$) is the ν_e ($\bar\nu_e$) spectral and angular distribution function, and $G(\omega,\mathbf{v}) = \mathrm{sgn}(\omega)[F_{\nu_e}(\omega,\mathbf{v}) - F_{\nu_x}(\omega,\mathbf{v})]/n_{\nu_e}$. The contraction $v^\rho(\mathbf{v})v_\rho(\mathbf{v}')$ gives the factor $(1-\mathbf{v}\cdot\mathbf{v}')$ that is explicitly included in the usual expression of $\mathsf{H}_{\nu\nu}(\mathbf{v})$. Here we emphasize the physical importance of J^ρ and will discuss neutrino flavor evolution using its 12 components.

We focus on the so-called fast flavor oscillations [9,10]. When the angular distribution $\int_{-\infty}^{+\infty} d\omega\, G(\omega,\mathbf{v})$ of the electron lepton number (νELN) carried by a dense neutrino gas has a zero-crossing, i.e., switches from being positive to negative, an instability may be triggered, which could result in fast flavor conversion on length scales as short as $\sim\mathcal{O}(1\text{ m})$ for conditions in neutron star mergers [11,12] and supernovae [13–15]. Whereas the above flavor instability can be identified by a linear stability analysis [5,6,16], the eventual outcome of fast oscillations is much harder to ascertain for realistic astrophysical environments. Apart from the uncertainties in modeling the neutrino emission in supernovae and neutron star mergers, numerical treatment of neutrino flavor evolution is further hampered by the complicated geometry and intrinsically dynamic nature of such environments. Consequently, studies of fast oscillations beyond the linear regime have been restricted to greatly simplified models so far. Specifically, Eq. (1) was solved for artificial νELN angular distributions by keeping the spatial derivative only in one [17–19] or two directions [20]. Other studies dropped either the time [21] or spatial derivative [22–24].

In this letter, we assume a homogeneous neutrino gas for which the spatial derivative can be ignored. We find the stationary solutions and compare them to the results from evolution calculations. We also discuss improvement of these solutions and their use as estimates of the effects of fast oscillations in astrophysical environments.

2. Stationary solutions

Under our assumption of homogeneity, Eq. (1) becomes

$$\partial_t \mathsf{P}(\omega,\mathbf{v}) = \mathsf{H}(\omega,\mathbf{v}) \times \mathsf{P}(\omega,\mathbf{v}). \tag{3}$$

The evolution of $\mathsf{P}(\omega,\mathbf{v})$ for the initial ν_e ($\omega > 0$) differs from that for the initial $\bar\nu_e$ ($\omega < 0$) only through the vacuum term $\mathsf{H}_{\rm vac}(\omega)$ in $\mathsf{H}(\omega,\mathbf{v})$. For the dense astrophysical environments of interest to us, $\mathsf{H}_{\rm vac}(\omega)$ can be ignored because the magnitude of ω is far less than that of λ or μ associated with $\mathsf{H}_{\rm mat}$ or $\mathsf{H}_{\nu\nu}(\mathbf{v})$, respectively. The effect of $\mathsf{H}_{\rm vac}(\omega)$ is to initiate neutrino flavor mixing, which can be approximated by allowing $\mathsf{P}(\omega,\mathbf{v})$ to have small initial deviations from the pure flavor states. With this prescription, the evolution of $\mathsf{P}(\omega,\mathbf{v})$ no longer depends on ω. We write $\mathsf{P}(\omega,\mathbf{v}) = \mathsf{P}(\mathbf{v})$ and solve the evolution equation

$$\partial_t \mathsf{P}(\mathbf{v}) = \mathsf{H}(\mathbf{v}) \times \mathsf{P}(\mathbf{v}), \tag{4}$$

where $\mathsf{H}(\mathbf{v}) = \lambda\hat{\mathbf{e}}_3 + v^\rho(\mathbf{v})\mathsf{J}_\rho$, $\mathsf{J}^\rho = \mu\int d\mathbf{v}'\, g(\mathbf{v}')v^\rho(\mathbf{v}')\mathsf{P}(\mathbf{v}')$, and $g(\mathbf{v}) = \int_{-\infty}^{+\infty} d\omega\, G(\omega,\mathbf{v})$ is the angular νELN distribution. From Eq. (4), we obtain $\partial_t \mathsf{J}^t = \lambda\hat{\mathbf{e}}_3 \times \mathsf{J}^t$. For the small initial deviations of $\mathsf{P}(\mathbf{v})$ from the pure flavor states, J^t is essentially parallel to $\hat{\mathbf{e}}_3$ initially (at $t = t_0$). Therefore, $\partial_t \mathsf{J}^t \approx 0$ and $\mathsf{J}^t \approx \mathsf{J}^t_{t_0} \approx \mu_{\rm eff}\hat{\mathbf{e}}_3$, where $\mu_{\rm eff} = \mu\int d\mathbf{v}\, g(\mathbf{v})$ is specified by the νELN.

Based on the above discussion, we take

$$\mathsf{H}(\mathbf{v}) = (\lambda + \mu_{\rm eff})\hat{\mathbf{e}}_3 - (v^x\mathsf{J}^x + v^y\mathsf{J}^y + v^z\mathsf{J}^z). \tag{5}$$

The components of the polarization current J^x, J^y, and J^z are vectors in the flavor space. At any specific time, the range of $\mathsf{H}(\mathbf{v})$ is determined by these vectors and the constraint $(v^x)^2 + (v^y)^2 + (v^z)^2 = 1$, and each $\mathsf{P}(\mathbf{v})$ precesses with the corresponding angular velocity $\mathsf{H}(\mathbf{v})$. We seek stationary solutions for which all polarization vectors collectively precess with the same angular velocity Ω on average. In the frame that co-rotates with these vectors, the evolution equation becomes

$$\tilde\partial_t \mathsf{P}(\mathbf{v}) = [\mathsf{H}(\mathbf{v}) - \Omega] \times \mathsf{P}(\mathbf{v}) = \mathsf{H}'(\mathbf{v}) \times \mathsf{P}(\mathbf{v}). \tag{6}$$

We assume adiabatic evolution, for which the angle between $\mathsf{P}(\mathbf{v})$ and $\mathsf{H}'(\mathbf{v}) = \mathsf{H}(\mathbf{v}) - \Omega$ stays fixed (see similar approach in [25,26]). Because of the constraint $\mathsf{J}^t \approx \mu_{\rm eff}\hat{\mathbf{e}}_3$, Ω is approximately parallel to $\hat{\mathbf{e}}_3$ for the stationary solutions. For the small initial deviations of $\mathsf{P}(\mathbf{v})$ from the pure flavor states, J^x, J^y, and J^z are also approximately parallel to $\hat{\mathbf{e}}_3$ at time t_0. So $\mathsf{P}(\mathbf{v})$ is parallel to $\mathsf{H}'(\mathbf{v})$ initially, and the adiabatic condition can be written as

$$\mathsf{P}(\mathbf{v}) = \epsilon(\mathbf{v})\hat{\mathsf{H}}'(\mathbf{v}), \tag{7}$$

where $\hat{\mathsf{H}}'(\mathbf{v})$ is the unit vector in the direction of $\mathsf{H}'(\mathbf{v})$, and

$$\epsilon(\mathbf{v}) = \mathrm{sgn}\left\{\hat{\mathbf{e}}_3 \cdot \left[\mathsf{H}_{t_0}(\mathbf{v}) - \Omega\right]\right\} = \mathrm{sgn}\left[H'_{3,t_0}(\mathbf{v})\right]. \tag{8}$$

The angular velocity Ω and the polarization current components J^x, J^y, and J^z for the stationary solutions can be solved iteratively by using Eqs. (7) and (8) in the definition of J^ρ and applying the constraint $\mathsf{J}^t \approx \mu_{\rm eff}\hat{\mathbf{e}}_3$. Clearly, it is most convenient to carry out the above procedure in the co-rotating frame.

3. Example solutions

We now illustrate the stationary solutions with specific examples. Because the angular velocity Ω is approximately parallel to the matter term $\lambda\hat{\mathbf{e}}_3$ in H, λ effectively shifts the magnitude of Ω. We take $\lambda = 0$ and $\mu = 10^4/(4\pi)$ km^{-1}. Motivated by the conditions in supernovae [27], we assume azimuthally symmetric νELN distributions $g(\mathbf{v}) = g(v^z)$, where

$$g(v^z) = \begin{cases} 1.25 - 0.25\gamma - (0.5+0.5\gamma)e^{-\left[(1-v^z)/0.7\right]^3}, \\ \quad 1 \le \gamma \le 2, \\ 1.25 - 0.25\gamma - 1.5e^{-\left[(1-v^z)/(0.3+0.2\gamma)\right]^3}, \\ \quad 2 < \gamma \le 3, \\ 2 - 0.5\gamma - (3-0.5\gamma)e^{-\left[(1-v^z)/(0.3\gamma)\right]^3}, \\ \quad 3 < \gamma \le 4. \end{cases} \tag{9}$$

The range of $\gamma = 1$–4 allows the above $g(v^z)$ to have any zero-crossing between $v^z = 1$ and -1 (see Fig. 1). We focus on the cases of $\gamma = 2$ and 3 with a crossing at $v^z \approx 0.38$ and 0.07, respectively.

We first solve Eq. (4) numerically using 600 bins for v^z and 320 bins for the azimuthal angle of $\mathbf{v}$. We have checked that convergence is achieved for this angular resolution. All polarization vectors $\mathsf{P}(\mathbf{v})$ are assigned random deviations between -10^{-3} and 10^{-3} from $P_3(\mathbf{v}) = 1$ at $t = t_0$. Their evolution is followed up to $t - t_0 = 2$ km, when an approximately stationary state has been reached (see Appendix A). The results on the survival probability $(P_3+1)/2$ for $\gamma = 2$ and 3 are shown in Figs. 2(b) and 3(b), respectively. Because the azimuthal symmetry is broken by the initial conditions adopted to approximate the effects of the vacuum term in $\mathsf{H}(\omega,\mathbf{v})$, these results depend on the azimuthal angle of $\mathbf{v}$ for each bin of v^z. The corresponding values of Ω, J^x, J^y, and J^z are given in Table 1.

We next calculate the stationary solutions as presented in Section 2. For all practical purposes, we can assume pure flavor

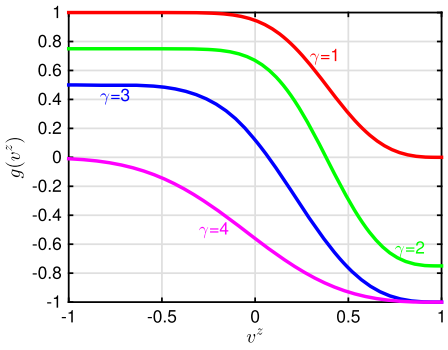

Fig. 1. The assumed νELN distributions $g(v^z)$. The range of $\gamma = 1$–4 allows any zero-crossing between $v^z = 1$ and -1.

Table 1
Characteristics of stationary solutions.

γ	results	Ω	$J_\perp^x$	$J_\perp^y$	$J_\perp^z$	J_3^x	J_3^z
2	numerical	3750	800	1200	1600	0	−2000
2	IIIa	4089	1392	1392	0	0	−2446
2	IVa	3705	462	154	2082	190	−1762
3	numerical	−870	650	650	0	0	−3200
3	IIIa	−900	799	799	0	0	−3108
3	IIIa′	−867	622	622	0	0	−3161

states to obtain $\mathsf{J}^t = \mu_{\rm eff}\hat{\mathbf{e}}_3$, $\mathsf{J}^x = \mathsf{J}^y = 0$, and $\mathsf{J}^z \parallel \hat{\mathbf{e}}_3$ at $t = t_0$, which gives $\mathsf{H}_{t_0}(\mathbf{v}) \parallel \hat{\mathbf{e}}_3$. Specifically, the initial conditions are $J_3^t = 2812$ km^{-1}, $J_3^z = -3030$ km^{-1} for $\gamma = 2$ and $J_3^t = -1028$ km^{-1}, $J_3^z = -3286$ km^{-1} for $\gamma = 3$. Conservation of J^t requires $\Omega = \Omega\hat{\mathbf{e}}_3$. Due to the azimuthal symmetry of $g(v^z)$ around the z axis in the Euclidean space, we can specify the x and y axes by setting $J_3^y = 0$ for the stationary solutions. In addition, the rotational symmetry around $\hat{\mathbf{e}}_3$ in the flavor space allows us to specify the directions $\hat{\mathbf{e}}_1$ and $\hat{\mathbf{e}}_2$ of the corotating frame by setting $J_2^x = 0$. The remaining components of the neutrino polarization current J_1^x, J_1^y, J_1^z, J_2^y, J_2^z, J_3^x, and J_3^z for the stationary solutions can be solved from the iterative procedure in Section 2.

We find that the stationary solutions can be classified into the following types, with the subscript $\perp$ denoting either $\hat{\mathbf{e}}_1$ or $\hat{\mathbf{e}}_2$: (I) $J_\perp^{x,y,z} \sim 0$, which represents the initial configuration, and therefore, is trivial, (II) $J_\perp^{x,y} \sim 0$ and $J_\perp^z \sim \mathcal{O}(\mu)$, (III) $J_\perp^{x,y} \sim \mathcal{O}(\mu)$ and $J_\perp^z \sim 0$, and (IV) $J_\perp^{x,y} \sim \mathcal{O}(\mu)$ and $J_\perp^z \sim \mathcal{O}(\mu)$. Type III is further divided into two subtypes: (IIIa) $\mathsf{J}_\perp^x \perp \mathsf{J}_\perp^y$ ($J_1^x \neq 0$, $J_1^y = 0$, $J_2^y \neq 0$), and (IIIb) $\mathsf{J}_\perp^x \parallel \mathsf{J}_\perp^y$ ($J_1^x \neq 0$, $J_1^y \neq 0$, $J_2^y = 0$). Similarly, type IV is further divided into three subtypes: (IVa) $\mathsf{J}_\perp^x \perp \mathsf{J}_\perp^y$ and $\mathsf{J}_\perp^x \parallel \mathsf{J}_\perp^z$ ($J_1^x \neq 0$, $J_1^y = 0$, $J_1^z \neq 0$, $J_2^y \neq 0$, $J_2^z = 0$), (IVb) $\mathsf{J}_\perp^x \parallel \mathsf{J}_\perp^y$ and $\mathsf{J}_\perp^y \perp \mathsf{J}_\perp^z$ ($J_1^x \neq 0$, $J_1^y \neq 0$, $J_1^z = J_2^y = 0$, $J_2^z \neq 0$), and (IVc) $\mathsf{J}_\perp^x \parallel \mathsf{J}_\perp^y \parallel \mathsf{J}_\perp^z$ ($J_1^x \neq 0$, $J_1^y \neq 0$, $J_1^z \neq 0$, $J_2^y = J_2^z = 0$). While the above classification reflects specific relations among the neutrino polarization current components, such relations are not used to find the stationary solutions but are observed after the solutions are obtained. Note that large magnitudes of $J_\perp^{x,y,z}$ correspond to substantial overall flavor transformation with large magnitudes of $P_\perp$ for wide ranges of $\mathbf{v}$.

Because the procedure outlined in Section 2 involves solving integral equations, the results are not unique in general and are only candidate stationary solutions. We perturb the polarization vectors $\mathsf{P}(\mathbf{v})$ of a candidate solution with random deviations of magnitude up to 10^{-3} and evolve them with Eq. (4) until the stability of the solution can be established or otherwise. The stable ones are selected as true stationary solutions. Note that the results may not be unique even after the above stability test.

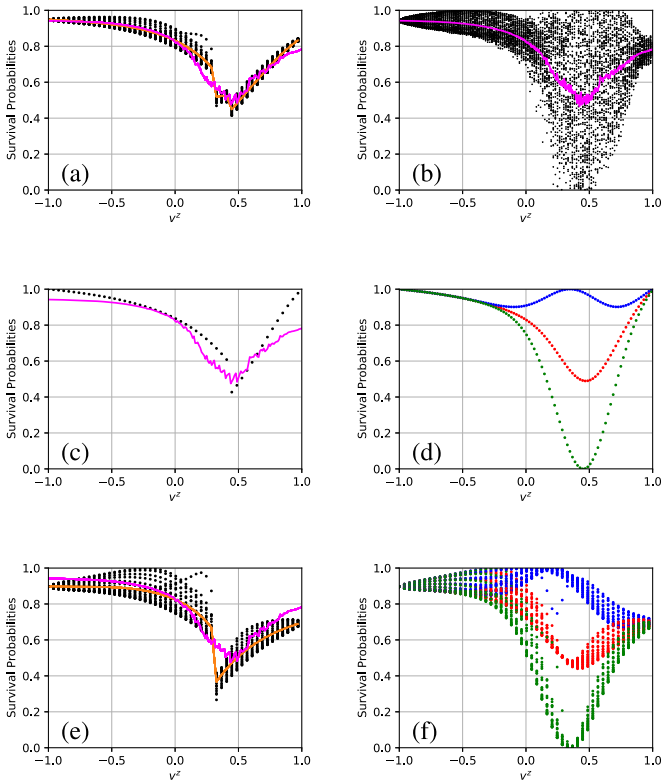

Fig. 2. Comparison of the survival probabilities from the stationary solutions with the numerical results for $\gamma = 2$. Symbols at the same v^z are for different azimuthal angles. In panel (a), the symbols are the averages of the results for the stationary solutions [shown in panels (c) and (e)] and the orange curve is obtained by averaging these symbols over the azimuthal angle. In panel (b), the symbols are the numerical results and the magenta curve is obtained by averaging these symbols over the azimuthal angle. The same magenta curve is also shown in panels (a), (c), and (e) for comparison. In panel (c), the symbols show the stationary solution of type IIIa. In panel (e), the symbols show the stationary solution of type IVa and the orange curve is obtained by averaging these symbols over the azimuthal angle. In panels (d) and (f), the symbols show the survival probabilities (red: mean, blue and green: limits) including the approximate effect of nonadiabatic evolution for the stationary solutions of types IIIa and IVa, respectively.

For $\gamma = 2$, we find seven candidate stationary solutions, two of which are stable (types IIIa and IVa). In contrast, only one of the five candidate solutions are stable (type IIIa) for $\gamma = 3$ (see Appendix A). The survival probabilities $(P_3 + 1)/2$ corresponding to the true stationary solutions are shown in Figs. 2 and 3 for comparison with the numerical results. The corresponding values of Ω, J^x, J^y, and J^z are given in Table 1. For both $\gamma = 2$ and 3, the stationary solution of type IIIa has $J_3^x = J_3^y = J_\perp^z = 0$ and $\mathsf{J}_\perp^x \perp \mathsf{J}_\perp^y$ with $J_\perp^x = J_\perp^y$. Consequently, $\hat{H}_3'$ and hence P_3 are independent of the azimuthal angle [see Eqs. (5) and (7)] with the corresponding survival probabilities exhibiting azimuthal symmetry. In contrast, for $\gamma = 2$, the stationary solution of type IVa has $J_3^x \neq 0$ and $J_\perp^{x,y,z} \neq 0$. Therefore, the corresponding survival probabilities depend on the azimuthal angle.

The νELN distribution $g(v^z)$ crosses zero at $v^z \approx 0.38$ and 0.07 for $\gamma = 2$ and 3, respectively. It can be seen from Figs. 2 and 3 that except for v^z near the zero-crossings, the survival probabilities given by the stationary solutions show the same trends as the numerical results. For more detailed comparisons, we calculate the average survival probability for each bin of v^z by averaging the numerical results over the azimuthal angle. Fig. 3(a) shows that the stationary solution for $\gamma = 3$ describes the average survival probabilities very well away from the zero-crossing. Because there are two types of stationary solutions for $\gamma = 2$, we calculate the corresponding average survival probability for each bin of

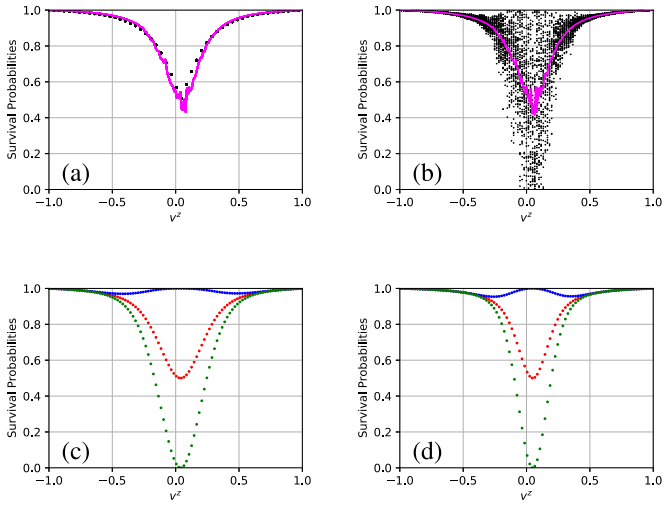

Fig. 3. Similar to Fig. 2, but for $\gamma = 3$. In panel (a), the symbols show the stationary solution of type IIIa and the magenta curve shows the survival probabilities averaged over the azimuthal angle for the numerical results in panel (b). In panel (c), the symbols show the survival probabilities (red: mean, blue and green: limits) including the approximate effect of nonadiabatic evolution based on the stationary solution in panel (a). Panel (d) is the same as panel (c), but for a new stationary solution of type IIIa′ characterized by a new ansatz for the neutrino polarization vectors.

v^z by weighing each type of solution equally and then averaging the results over the azimuthal angle. Fig. 2(a) shows that these average survival probabilities are also in good agreement with the numerical results away from the zero-crossing.

The large deviations of the survival probabilities for the stationary solutions from the numerical results for v^z near the zero-crossings are caused by the breakdown of adiabatic evolution assumed in deriving these solutions. The corresponding neutrinos have small values of $|\mathsf{H}'_{t_0}(\mathbf{v})| = |H'_{3,t_0}(\mathbf{v})| \ll \mu$ that result in nonadiabatic flavor evolution. The effect of this nonadiabaticity can be approximated by including a component of $\mathsf{P}(\mathbf{v})$ that is perpendicular to and rapidly rotating around $\mathsf{H}'(\mathbf{v})$ in addition to the component aligned with the latter and given by

$$\mathsf{P}_{\rm align}(\mathbf{v}) \approx \epsilon_{\rm eff}(\mathbf{v})\hat{\mathsf{H}}'(\mathbf{v}). \tag{10}$$

In the above equation, $\hat{\mathsf{H}}'(\mathbf{v})$ is taken from the stationary solution and $\epsilon_{\rm eff}(\mathbf{v})$ is taken as the error function

$$\epsilon_{\rm eff}(\mathbf{v}) = {\rm erf}\left[H'_{3,t_0}(\mathbf{v})/\mu\right], \tag{11}$$

which approaches $\epsilon(\mathbf{v}) = \pm 1$ in Eq. (8) for adiabatic evolution with $|H'_{3,t_0}/\mu| \gg 1$. Because the magnitude of $\mathsf{P}(\mathbf{v})$ is conserved during the evolution, its component perpendicular to $\mathsf{H}'(\mathbf{v})$ should have a magnitude of $\sqrt{1-[\epsilon_{\rm eff}(\mathbf{v})]^2}$. Due to the rapid rotation of this component around $\mathsf{H}'(\mathbf{v})$, the effective P_3 oscillates between the limits

$$P_{3,\rm lim}(\mathbf{v}) = \bar{P}_3(\mathbf{v}) \pm \sqrt{1-[\epsilon_{\rm eff}(\mathbf{v})]^2}\sqrt{1-[\hat{H}'_3(\mathbf{v})]^2}\,, \tag{12}$$

where

$$\bar{P}_3(\mathbf{v}) = P_{3,\rm align}(\mathbf{v}) \approx \epsilon_{\rm eff}(\mathbf{v})\hat{H}'_3(\mathbf{v}) \tag{13}$$

is the mean value due to the component aligned with $\mathsf{H}'(\mathbf{v})$. The corresponding survival probabilities are shown as the blue, green (limits), and red (mean) symbols in Figs. 2(d), 2(f) for $\gamma = 2$ and in Fig. 3(c) for $\gamma = 3$. It can be seen that these results describe both the trends and the range of the numerical results rather well.

Because the rapidly rotating component of $\mathsf{P}(\mathbf{v})$ perpendicular to $\mathsf{H}'(\mathbf{v})$ is essentially averaged out, only $\mathsf{P}_{\rm align}(\mathbf{v})$ is effectively used to find the stationary solutions. We can choose $\epsilon_{\rm eff}(\mathbf{v})$ and use Eq. (10) to replace Eq. (8) in the procedure to find these solutions. As an example, we choose

$$\epsilon'_{\rm eff}(\mathbf{v}) = {\rm erf}\left[1.5H'_{3,t_0}(\mathbf{v})/\mu\right] \tag{14}$$

for $\gamma = 3$ and obtain a new stationary solution, which is also of type IIIa (denoted as IIIa′). The corresponding survival probabilities (mean and limits) are calculated in the same way as for Fig. 3(c) and shown in Fig. 3(d). The corresponding values of Ω, J^x, J^y, and J^z are given in Table 1. It can be seen that the new stationary solution is much closer to the numerical results. While the effect of nonadiabatic evolution can be well approximated by choosing an appropriate $\epsilon'_{\rm eff}(\mathbf{v})$ as in the above example, we note, however, that our original procedure to find the stationary solutions assuming adiabatic evolution is more straightforward and can already produce average survival probabilities to good approximation.

As discussed above, nonadiabatic evolution appears to be associated with the zero-crossing of the νELN distribution $g(v^z)$. On the other hand, if $g(v^z)$ has no zero-crossing as for $\gamma = 1$ or 4 (see Fig. 1), the initial values of $P_3(\mathbf{v}) = 1$ make J^t_3 reach the most positive or negative value for $\gamma = 1$ or 4, respectively. Conservation of J^t_3 then ensures $P_3(\mathbf{v}) = 1$ subsequently, and therefore, there is no flavor evolution at all [5].

4. Discussion and conclusions

We have presented a method to find the stationary solutions for fast flavor oscillations of a homogeneous dense neutrino gas whose angular νELN distribution has a zero-crossing. These solutions correspond to collective precession of all neutrino polarization vectors around a fixed axis in the flavor space on average, and are conveniently studied in the co-rotating frame. We have shown that these solutions can account for the numerical results of explicit evolution calculations, and that even with the simplest assumption of adiabatic evolution, they can provide the average survival probabilities to good approximation. These solutions can be further improved by including the effect of nonadiabatic evolution, which in turn, can be approximated by choosing an appropriate ansatz for the alignment of the polarization vectors with the effective Hamiltonian in the co-rotating frame. While we have focused on specific νELN distributions for our examples, we show in Appendix B that our method applies to other νELN distributions as well.

Besides shedding light on the nonlinear regime of fast oscillations, the stationary solutions discussed here provide physically motivated estimates of the average survival probabilities beyond the simple limit of complete flavor equilibration. Because these solutions can be efficiently calculated, they may be incorporated in simulations of dynamical astrophysical environments such as supernovae and neutron star mergers, for which the computational resources must be almost exclusively devoted to hydrodynamics and regular neutrino transport by necessity. We note that our method assumes a homogeneous neutrino gas but the environments where fast oscillations may occur are most likely inhomogeneous. Consequently, the stationary solutions discussed here may only provide a crude yet efficient way to explore the effects of fast oscillations on neutrino-related processes in supernovae and neutron star mergers. The general problem of flavor evolution of an inhomogeneous dense neutrino gas is beyond our scope here and requires further dedicated studies.

Declaration of competing interest

The authors declare that they have no known competing financial interests or personal relationships that could have appeared to influence the work reported in this paper.

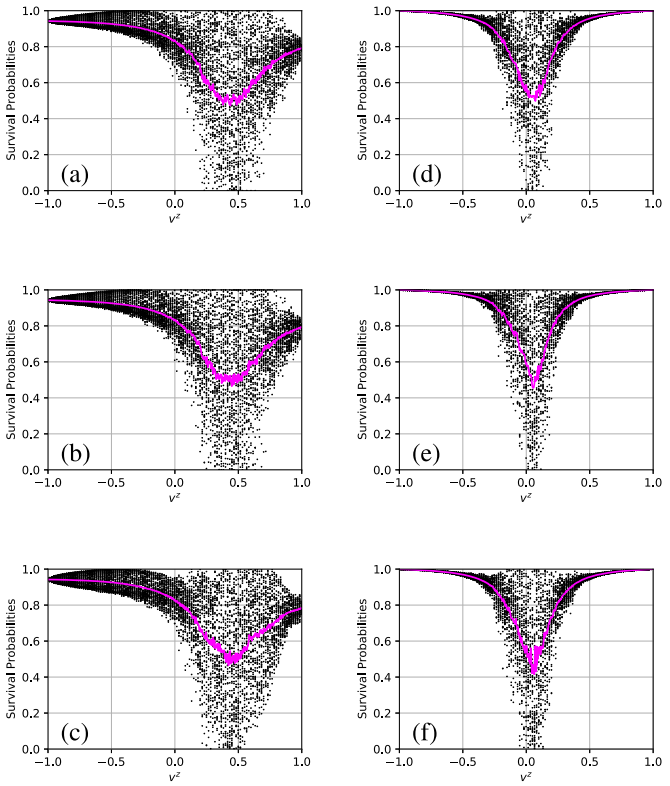

Fig. A.4. Snapshots of survival probabilities. Panels (a), (b), and (c) [(d), (e), and (f)] are for $t = 1.6$, 1.8, and 2 km, respectively, for the νELN distribution with $\gamma = 2$ (3).

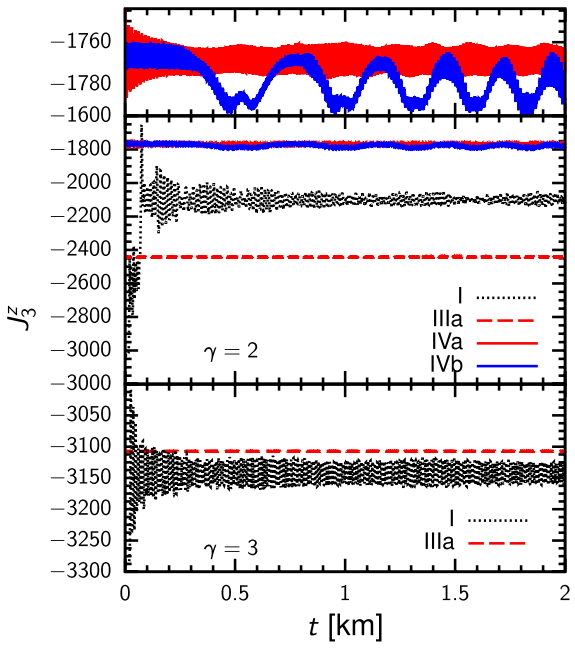

Fig. A.5. Evolution of J_3^z for some candidate stationary solutions after they are perturbed. For the νELN distribution with $\gamma = 2$, the difference between types IVa and IVb is highlighted in the top panel.

Acknowledgements

This work was supported in part by the US Department of Energy [DE-FG02-87ER40328]. We thank the anonymous referee for constructive criticisms and helpful suggestions. Z. X. was partly supported by the European Research Council (ERC) under the European Union's Horizon 2020 research and innovation programme (ERC Advanced Grant KILONOVA No. 885281). Some calculations were carried out at the Minnesota Supercomputing Institute.

Appendix A. Numerical tests

Fig. A.4 shows the snapshots of our explicit evolution calculations at $t = 1.6$, 1.8, and 2 km for the assumed νELN distributions with $\gamma = 2$ and 3. It can be seen that an approximately stationary state has been reached by $t = 2$ km in both cases.

Fig. A.5 shows the evolution of J_3^z for some candidate stationary solutions after they are perturbed. Note that the results for type I are calculated from the initial configurations and become approximately constant at late times as expected of the approximately stationary states shown in Fig. A.4. For $\gamma = 2$, only types IIIa and IVa are the true stationary solutions. Type IVb is quasi-stable for $t < 0.3$ km but deviates from the initial state subsequently. Therefore, it is not a true stationary solution. Note that the average value of J_3^z for types IIIa and IVa is close to the late-time value of J_3^z for type I. For $\gamma = 3$, only type IIIa is the true stationary solution.

Appendix B. Other νELN distributions

We have repeated the calculations for two more νELN distributions taken from [24] (case A) and [6] (case B):

$$g_A(v^z) = -\exp\left[-\frac{(\cos^{-1} v^z)^2}{2}\right] + 0.5, \tag{B.1}$$

$$g_B(v^z) = 10\exp\left[-\frac{(1-v^z)^2}{0.72}\right] - 10.66\exp\left[-\frac{(1-v^z)^2}{0.562}\right]. \tag{B.2}$$

The zero-crossing occurs at $v^z \approx 0.38$ and 0.6 for $g_A(v^z)$ and $g_B(v^z)$, respectively.

Fig. B.6 shows that an approximately stationary state has been reached by $t = 2$ km for the explicit evolution calculations for both cases A and B, and compares the survival probabilities from the stationary solutions with the numerical results. For case A, we find three nontrivial candidate stationary solutions of types II, IIIb, and IVb. Only type IVb is stable (see Fig. B.7), and the corresponding average survival probabilities match the numerical results very well away from the zero-crossing at $v^z \approx 0.38$ [see Fig. B.6(d)]. The trend and range of the numerical results can also be explained by including the approximate effect of nonadiabatic evolution based on this solution with

$$\epsilon_{\rm eff}(\mathbf{v}) = \mathrm{erf}\left[2H'_{3,t_0}(\mathbf{v})/\mu\right] \tag{B.3}$$

replacing Eq. (11) [see Fig. B.6(e)]. For case B, we find two nontrivial candidate stationary solutions of types IIIa and IIIb. Only type IIIa is stable (see Fig. B.7). The corresponding average survival probabilities qualitatively follow the numerical results away from the zero-crossing at $v^z \approx 0.6$ [see Fig. B.6(i)]. The trend and range of the numerical results for $v^z \gtrsim 0.5$ can also be explained by including the approximate effect of nonadiabatic evolution based on this solution with

$$\epsilon_{\rm eff}(\mathbf{v}) = \mathrm{erf}\left[3H'_{3,t_0}(\mathbf{v})/\mu\right] \tag{B.4}$$

replacing Eq. (11) [see Fig. B.6(j)].

The flavor evolution for the νELN distribution of case B differs from all the other cases considered in that it is associated with a sign flip of J_3^z. As J_3^z changes from the initial value of $-803\,\mathrm{km}^{-1}$ to $\approx 450\,\mathrm{km}^{-1}$ for the approximately stationary state (see Fig. B.7), neutrinos with a wide range of v^z undergo nonadiabatic evolution. This effect cannot be captured by our approximate treatment of nonadiabatic evolution, which is appropriate only for a limited

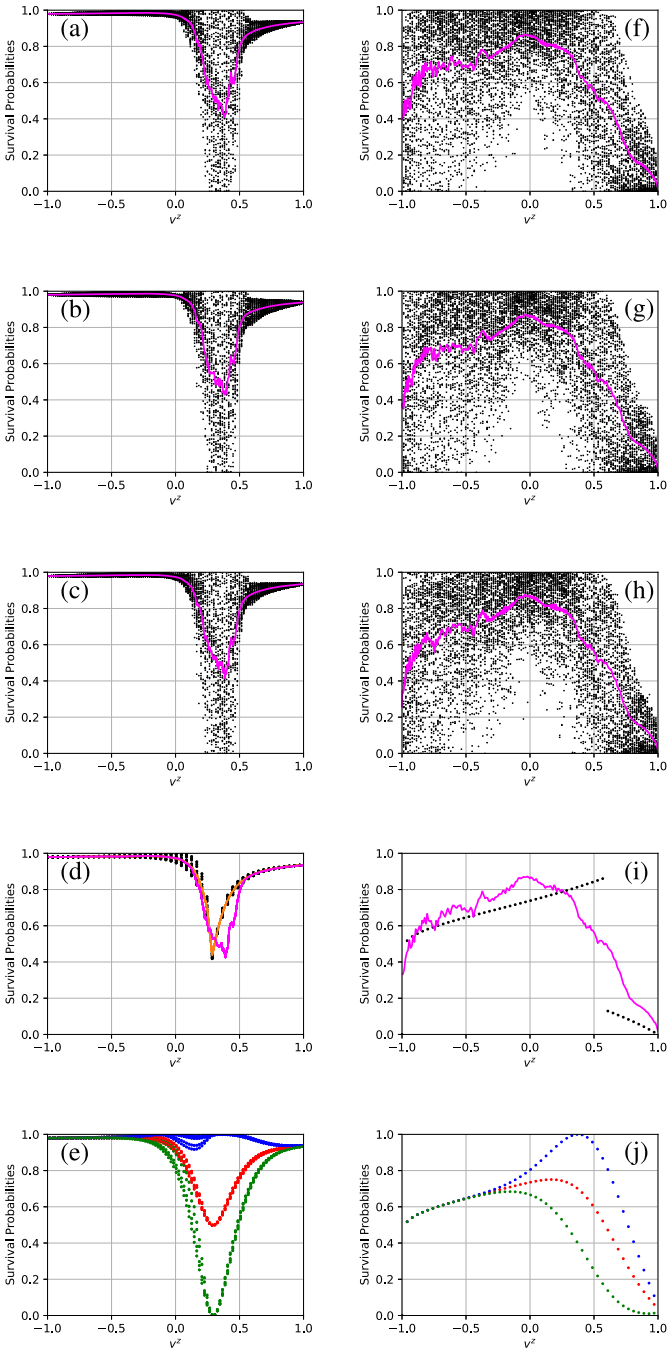

Fig. B.6. Comparison of the survival probabilities from the stationary solutions with the numerical results for the νELN distributions of cases A and B. Symbols at the same v^z are for different azimuthal angles. In panels (a), (b), and (c), snapshots of the numerical results are shown for $t = 1.6$, 1.8, and 2 km, respectively, for case A. The magenta curves are the survival probabilities averaged over the azimuthal angle. In panel (d), the symbols show the stationary solution for case A, the orange curve is obtained by averaging these symbols over the azimuthal angle, and the magenta curve is the same as that in panel (c). In panel (e), the symbols show the survival probabilities (red: mean, blue and green: limits) including the approximate effect of nonadiabatic evolution for the stationary solution for case A. Panels (f)–(j) are similar to panels (a)–(e), but for case B.

range of v^z around the zero-crossing. We note, however, that for the likely inhomogeneous astrophysical environments, the dominant instability associated with the νELN distribution of case B grows differently on different spatial scales [6,17]. Therefore, a realistic treatment of this case must address both the temporal and

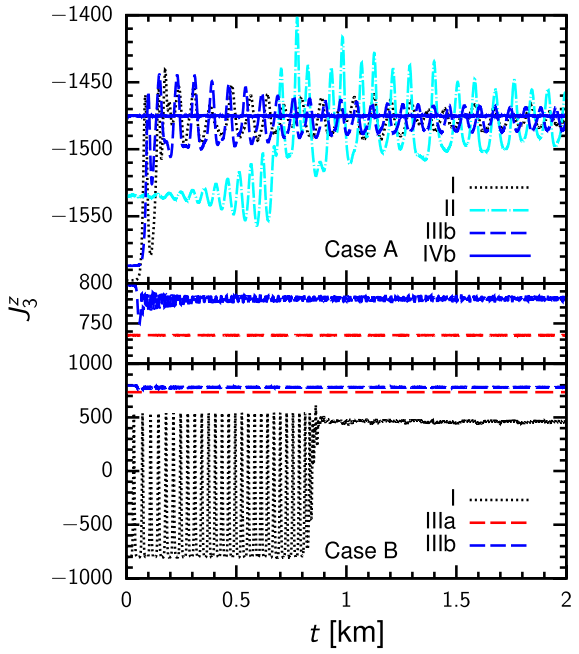

Fig. B.7. Evolution of J_3^z for the candidate stationary solutions for the νELN distributions of cases A and B after they are perturbed. For case B, the difference between types IIIa and IIIb is highlighted in the middle panel.

spatial flavor evolution of neutrinos, which is beyond our scope here.

References

[1] K.A. Olive, et al., Review of particle physics, Chin. Phys. C 38 (9) (2014) 090001.
[2] H. Duan, G.M. Fuller, Y.-Z. Qian, Collective neutrino oscillations, Annu. Rev. Nucl. Part. Sci. 60 (2010) 569–594, https://doi.org/10.1146/annurev.nucl.012809.104524.
[3] G. Raffelt, S. Sarikas, D. de Sousa Seixas, Axial symmetry breaking in self-induced flavor conversion of supernova neutrino fluxes, Phys. Rev. Lett. 111 (9) (2013) 091101, https://doi.org/10.1103/PhysRevLett.111.091101.
[4] S. Chakraborty, R. Hansen, I. Izaguirre, G. Raffelt, Collective neutrino flavor conversion: recent developments, Nucl. Phys. B 908 (2016) 366–381, https://doi.org/10.1016/j.nuclphysb.2016.02.012.
[5] I. Izaguirre, G. Raffelt, I. Tamborra, Fast pairwise conversion of supernova neutrinos: a dispersion relation approach, Phys. Rev. Lett. 118 (2) (2017) 021101, https://doi.org/10.1103/PhysRevLett.118.021101.
[6] C. Yi, L. Ma, J.D. Martin, H. Duan, Dispersion relation of the fast neutrino oscillation wave, Phys. Rev. D 99 (6) (2019) 063005, https://doi.org/10.1103/PhysRevD.99.063005.
[7] J.D. Martin, S. Abbar, H. Duan, Nonlinear flavor development of a two-dimensional neutrino gas, Phys. Rev. D 100 (2) (2019) 023016, https://doi.org/10.1103/physrevd.100.023016.
[8] J.D. Martin, J. Carlson, H. Duan, Spectral swaps in a two-dimensional neutrino ring model, Phys. Rev. D 101 (2) (2020) 023007.
[9] R.F. Sawyer, Speed-up of neutrino transformations in a supernova environment, Phys. Rev. D 72 (4) (2005) 045003, https://doi.org/10.1103/PhysRevD.72.045003.
[10] R. Sawyer, Multiangle instability in dense neutrino systems, Phys. Rev. D 79 (10) (2009) 105003, https://doi.org/10.1103/PhysRevD.79.105003.
[11] M.-R. Wu, I. Tamborra, Fast neutrino conversions: ubiquitous in compact binary merger remnants, Phys. Rev. D 95 (10) (2017) 103007, https://doi.org/10.1103/PhysRevD.95.103007.
[12] M.-R. Wu, I. Tamborra, O. Just, H.-T. Janka, Imprints of neutrino-pair flavor conversions on nucleosynthesis in ejecta from neutron-star merger remnants, Phys. Rev. D 96 (12) (2017) 123015, https://doi.org/10.1103/PhysRevD.96.123015.
[13] B. Dasgupta, A. Mirizzi, M. Sen, Fast neutrino flavor conversions near the supernova core with realistic flavor-dependent angular distributions, J. Cosmol. Astropart. Phys. 2017 (02) (2017) 019, https://doi.org/10.1088/1475-7516/2017/02/019.
[14] I. Tamborra, F. Hanke, H.-T. Janka, B. Müller, G.G. Raffelt, A. Marek, Self-sustained asymmetry of lepton-number emission: a new phenomenon during the supernova shock-accretion phase in three dimensions, Astrophys. J. 792 (2) (2014) 96, https://doi.org/10.1088/0004-637X/792/2/96.

[15] T. Morinaga, H. Nagakura, C. Kato, S. Yamada, Fast neutrino-flavor conversion in the preshock region of core-collapse supernovae, Phys. Rev. Res. Int. 2 (1) (2020) 012046.
[16] B. Dasgupta, A. Mirizzi, M. Sen, Simple method of diagnosing fast flavor conversions of supernova neutrinos, Phys. Rev. D 98 (10) (2018) 103001, https://doi.org/10.1103/PhysRevD.98.103001.
[17] J.D. Martin, C. Yi, H. Duan, Dynamic fast flavor oscillation waves in dense neutrino gases, Phys. Lett. B 800 (2020) 135088, https://doi.org/10.1016/j.physletb.2019.135088.
[18] S. Bhattacharyya, B. Dasgupta, Late-time behavior of fast neutrino oscillations, Phys. Rev. D 102 (6) (2020) 063018.
[19] S. Bhattacharyya, B. Dasgupta, Fast flavor depolarization of supernova neutrinos, Phys. Rev. Lett. 126 (6) (2021) 061302.
[20] S. Shalgar, I. Padilla-Gay, I. Tamborra, Neutrino propagation hinders fast pairwise flavor conversions, J. Cosmol. Astropart. Phys. 2020 (06) (2020) 048, https://doi.org/10.1088/1475-7516/2020/06/048.
[21] S. Abbar, M.C. Volpe, On fast neutrino flavor conversion modes in the nonlinear regime, Phys. Lett. B 790 (2019) 545–550, https://doi.org/10.1016/j.physletb.2019.02.002.
[22] L. Johns, H. Nagakura, G.M. Fuller, A. Burrows, Neutrino oscillations in supernovae: angular moments and fast instabilities, Phys. Rev. D 101 (4) (2020) 043009.
[23] L. Johns, H. Nagakura, G.M. Fuller, A. Burrows, Fast oscillations, collisionless relaxation, and spurious evolution of supernova neutrino flavor, Phys. Rev. D 102 (10) (2020) 103017.
[24] S. Shalgar, I. Tamborra, Dispelling a myth on dense neutrino media: fast pairwise conversions depend on energy, J. Cosmol. Astropart. Phys. 2021 (01) (2021) 014.
[25] H. Duan, G.M. Fuller, Y.-Z. Qian, Simple picture for neutrino flavor transformation in supernovae, Phys. Rev. D 76 (2007) 085013, https://doi.org/10.1103/PhysRevD.76.085013.
[26] M.-R. Wu, H. Duan, Y.-Z. Qian, Physics of neutrino flavor transformation through matter–neutrino resonances, Phys. Lett. B 752 (2016) 89–94.
[27] S. Abbar, H. Duan, K. Sumiyoshi, T. Takiwaki, M.C. Volpe, Fast neutrino flavor conversion modes in multidimensional core-collapse supernova models: the role of the asymmetric neutrino distributions, Phys. Rev. D 101 (4) (2020) 043016, https://doi.org/10.1103/PhysRevD.101.043016.